International Journal of Control, Automation and Systems 19(4) (2021) 1703-1714
http://dx.doi.org/10.1007/s12555-020-0015-7
ISSN:1598-6446 eISSN:2005-4092
http://www.springer.com/12555

Bearing Fault Online Identification Based on ANFIS

Nang Toan Truong, Tae-Il Seo, and Sy Dzung Nguyen*

Abstract: Effectiveness of online bearing status monitoring (OBSM) depends deeply on the online data processing ability and the sensitivity of data features used to recognize the mechanical-system dynamic response change. Focusing on these, we present a novel method of OBSM based on singular spectrum analysis (SSA) and adaptive neuro-fuzzy inference system (ANFIS) with the highlights as follows. A sensitive and stable multi-feature is discovered to better the ability to distill the valuable information in noisy and massive databases (NMDs) and process impulse-noise in them. The SSA-based high-frequency noise removal solution, the ANFIS' interpolating and identifying capability, and the dual function of the proposed multi-feature are combined in a new algorithm named AfOBSM for building a system of OBSM through two phases, offline and online. The offline is to identify the mechanical-system in the presence of the typical kinds of bearing faults. The ANFIS is trained in this phase using a training dataset. Meanwhile, the online is to estimate online the real status of the bearing(s) based on the trained ANFIS and a monitoring dataset. Surveys from an experimental-system were performed. The obtained results showed the positive effects of the AfOBSM.

Keywords: ANFIS-based fault diagnosis, bearing fault diagnosis, machine health monitoring, online damge identification.

1. INTRODUCTION

Fault online identification to exploit systems proactively and safely is a meaningful task that has been considered in many different types of systems [1–22]. It could be monitoring the status of Petri-nets based models depicting manufacturing systems, software programs, or communication networks [1,2]. It could also be the diagnosing faults on continuous-time systems or discrete-time systems [3–5], or managing the health of mechanical structures [7,8,19–22]. Based on the approach way, fault identification methods can be classified into two groups, structured and unstructured. Unlike the first group to fully know the system to describe, the second group pays attention to solving the inverse problem described by the system's dynamic feedback signal only. As a highly practical approach, it has attracted many researchers [1–23]. To build a reliable unstructured model, reality has shown that along with choosing an appropriate identification model and providing effective solutions for filtering noise, finding a feature stable and sensitive enough to distill valuable information in data is an especially vital work [7,8,10–16,23]. These inspire us to build a novel method of OBSM.

Noise from various sources such as measurement errors, false observations, external disturbances, or unspecified random aspects, etc., always exists in measurement data [24–30]. In which, impulse noise comes from internal or external unknown random factors. This is a type of electromagnetic interference normally existing in sensor-based measurement data. Because the formation situations and the mechanism of action on the measurement accuracy are unknown, and its source is unclear and not easily found [31], filtering random-valued impulse noise (IN) in NMDs has always been a challenge [24]. Some filtering methods, including the famous Kalman filter [32,33], had to rely on the assumption that their state variables were normal probability distributions. The difference between the actual and assumed data distribution was the reason for blurring their efficiency in filtering in [34]. Other approaches independent of the data distribution have been proposed [7,8,24,34–38]. In which, the mean filters [35–38] relied on the mean value of signals in a neighborhood called a window. Although the mean filters

Manuscript received February 1, 2020; revised May 26, 2020; accepted July 21, 2020. Recommended by Associate Editor Xiao-Heng Chang under the direction of Editor Guang-Hong Yang. The authors are very grateful to the reviewers for their useful comments and suggestions. This research is funded by Vietnam National Foundation for Science and Technology Development (NAFOSTED) under grant number 107.01-2019.328.

Nang Toan Truong is with the Faculty of Electronics Technology, Industrial University, Ho Chi Minh City, Vietnam (e-mail: truongnangtoan@iuh.edu.vn). Tae-Il Seo is with the Department of Mechanical Engineering, Incheon National University, Incheon, Korea (e-mail: tiseo@inu.ac.kr). Sy Dzung Nguyen is with Division of Computational Mechatronics, Institute for Computational Science, Ton Duc Thang University, Ho Chi Minh City, Viet Nam; Faculty of Electrical and Electronics Engineering, Ton Duc Thang University, Ho Chi Minh City, Viet Nam (e-mail: nguyensydung@tdtu.edu.vn).
* Corresponding author.

could outperform the normal-distribution based filters in the case of facing IN, there existed also disadvantages related to the formation of the window. Setting up the window with a low size to maintain the local attributes of the signal [38] may result in a significant increase in the computational cost, especially when dealing with NMDs with expanded data spaces. Whereas, determining the optimal window size is always a challenge. Different from the above time-domain based methods, SSA can be employed as a tool for analyzing in the frequency domain [22, 23]. Based on SSA, one can recognize the trend of the original signal if the vibration frequency of the structure is known. This property is useful for building a faster data processing mechanism. Also, by taking the noteworthy that the mechanical vibration concentrates most of its power on the low-frequency ranges, one can remove the high-frequency ranges. More especially, SSA can collaborate well with ANFIS. It should be noted that a combination of fuzzy logic [14] and artificial neural networks [16, 39] in the form of ANFIS could be done to get the enhanced advantages [24–30]. The collaboration of SSA and ANFIS, therefore, is a promising option to synchronize the phases of data-processing, identification, and prediction effectively.

An important mechanical property exploited to build unstructured fault identification models is that when a fault occurs in the mechanical system, its dynamic response is changed [10–20]. Signals to identify this change are not only obvious physical parameters such as vibration frequency, amplitude, or mode shape but also mathematical factors that hide the physical properties of the system [7, 11]. The aforementioned physical or mathematical parameters are often called features. To ensure reliability, the features must be stable and sensitive enough to the change in system dynamic response deriving from the faults but not sensitive to noise [17, 19]. The stable attribute here requires that, if the system is undamaged, there is no significant change in the value of the feature; otherwise, if the fault varying trend is maintained, the corresponding feature change trend must be preserved. Along with the feature attributes, the choice between structures of the feature should also be considered. Based on the structure, it can be separated into two groups, single-features [11, 12, 19] and multi-features [15, 18]. Single-features are built upon the individual variability of a single physical quantity, such as frequency, amplitude, mode shape, etc., to describe. Although the computational cost is low, the single-feature based methods are only suitable for simple systems with narrow dynamic varying ranges. In contrast, the multi-features exploit the consequences of the interactions of many variable quantities, such as geometric dimensions, frequencies, amplitudes, elastic modulus, inertia moments, phase oscillations, etc. Actually, any damage in a mechanical system causes most of the system's dynamic response parameters to be changed. So, such an approach is more natural, and it reflects systematic status more objectively. However, the multi-feature building faces significant challenges because it is difficult to recognize the relevance of each quantity explicitly in such a dynamic relationship. Besides, higher computational pressure is an issue for online applications. Although facing these difficulties, its comparative advantage of sensitivity has attracted researchers [7, 8, 11, 15, 18].

In [11], vibration signals from multiple sensors mounted in different positions were used to diagnose online bearing errors. Due to the instability of the links, the reliability of the data streams measured from the sensors is significantly different. A full review of the sensitivity differences for multiple channels was implemented to select the best data stream joining the training database at each time. Based on the training and historical databases and the K-nearest neighbor method, a framework of the fault diagnosis was set up. The channel selection like this could reduce the effect of system errors but could not cancel the negative effect of random-valued impulse noise, nor did it replace the role of the noise filter. Other approaches can be referred to in [7, 8], where online damage management methods were set up based on the solutions for data pre-processing and the interpolation capabilities of artificial intelligence (AI). In [7], the method relied on AI and a multi-feature model to estimate the status of bearings. In the case of the high data reliability, this was a promising method for distilling valuable information. However, its effectiveness might be blurred when facing IN and expanded data space size. Also, it often resulted in high computational pressure, required a hardware configuration to be strong enough. In [8], a combination of SSA and ANFIS was addressed to create new competencies in online data processing, analyzing, and identifying the change in system dynamic response. This was a meaningful collaboration, however, such SSA-based filtering took part in the high-frequency noise range only.

Inspired by the aforementioned issues, our motivation in this study is as follows:

1) Seeking solutions for filtering noise in all frequency bands and neutralizing the negative effects of IN;

2) Building a multi-feature with comparative advantages to perform OBSM well.

Specifically, we present a new multi-feature owning a dual function to distill valuable information in NMD. Together with taking the main role in recognizing the status of bearings based on the system's dynamic response, the multi-feature can blur the negative effect of IN and white noise but not lose the data local characteristics. The SSA-based solution for cancellation of high-frequency noise of [8] and the dual function of the multi-feature are exploited to process data. A combination of SSA, the multi-feature, and ANFIS is presented in a proposed new algorithm named AfOBSM for building a system of OBSM. It operates in two phases, the offline and online. An ANFIS is

trained in the offline to identify the mechanical-system in the presence of the typical kinds of bearing faults. Meanwhile, the real status of the bearings is recognized in the online relied on the trained ANFIS and online-measured databases.

The two main contributions are as follows: The first is the discovered multi-feature model. It owns the stability and dispersion attributes as detailed in Section 3, and also takes the role of a filter as mentioned in Remark 1. The second is the multi-feature based AfOBSM for online recognizing the system's real status. This aspect is presented in Section 4. Via the proposed multi-feature, the difference in the way of exploiting ANFIS, SSA, or their combination makes advantages of the AfOBSM comparing with the previous works [8,19] or the other one [7]. The method is not sensitive to noise and the data size. These are verified via real surveys in Section 5.

2. RELATED WORKS

2.1. Approximating a mapping by an ANFIS

Let consider a set of input-output data points $(\bar{\mathbf{x}}_i, y_i)$, $\bar{\mathbf{x}}_i = [x_{i1}, ..., x_{in}] \in \Re^n$, $y_i \in \Re^1$, $i = 1, ..., P$, depicting an unknown mapping $f : \mathrm{X} \to \mathrm{Y}$. For this work, the set is separated into C clusters to make fuzzy inference laws. The h-th fuzzy inference law is as follows:

$$R^{(h)} : \text{IF } x_{i1} \text{ is } A_1^h, \ ..., \text{AND } x_{in} \text{ is } A_n^h \text{ THEN } y_i^h \text{ is } B^h. \tag{1}$$

In the above, A_l^h, $l = 1, ..., n$, is the input fuzzy set while B^h is the corresponding output fuzzy set; 'x_{il} is A_l^h' is reflected by the relationship value $\mu_{A_l^h}(x_{il})$ of x_{il} belonging to A_l^i. For the center-average defuzzification and the product law, the output of the i-th data point is calculated as (2) or (3).

$$\hat{y}_i = \left(\sum_{h=1}^{M} y_i^{(h)} \prod_{l=1}^{n} \mu_{A_l^h}(x_{il}) \right) / \sum_{h=1}^{M} \prod_{l=1}^{n} \mu_{A_l^h}(x_{il}), \tag{2}$$

$$\hat{y}_i \equiv \hat{y}(\bar{x}_i) = \phi^T \lambda(\bar{x}_i); \tag{3}$$

$$\phi = [y^{(1)}, ..., y^{(M)}]^T; \quad \lambda(\bar{x}_i) = [\lambda^{(1)}(\bar{x}_i), ..., \lambda^{(M)}(\bar{x}_i)]^T;$$

$$\lambda^{(h)}(\bar{\mathbf{x}}_i) = \left(\prod_{l=1}^{n} \mu_{A_l^h}(x_{il}) \right) / \sum_{h=1}^{M} \prod_{l=1}^{n} \mu_{A_l^h}(x_{il}). \tag{4}$$

2.2. Singular spectrum analysis

SSA is described by three steps as follows [22]:

Step 1 (Embedding)**:** From a given time series of N_0 data points $(z_0, ..., z_{N_0-1})$ and a window length L_0, $1 < L_0 < N_0$, $K = N_0 - L_0 + 1$ sliding vectors $\mathbf{X}^j = (z_{j-1}, ..., z_{j+L_0-2})^T$, $j = 1, ..., K$, and a trajectory matrix $\mathbf{X}$ are defined:

$$\mathbf{X} = \begin{pmatrix} z_0 & z_1 & \cdots & z_{N_0-L_0} \\ z_1 & z_2 & \cdots & z_{N_0-L_0+1} \\ \vdots & \vdots & \ddots & \vdots \\ z_{L_0-1} & z_{L_0} & \cdots & z_{N_0-1} \end{pmatrix}. \tag{5}$$

Step 2 (Building the trajectory matrix)**:** One calculates the eigenvalues and eigenvectors of $\mathbf{S} = \mathbf{X}\mathbf{X}^T \in \Re^{L_0 \times L_0}$. Let $\lambda_1, ..., \lambda_d$ be the non-zero eigenvalues of $\mathbf{S}$ arranged in the descending order, and $\mathbf{U}_1, ..., \mathbf{U}_d$ be the corresponding eigenvectors. Vectors $\mathbf{V}_i$ are then constructed, $\mathbf{V}_i = \mathbf{X}^T\mathbf{U}_i/\sqrt{\lambda_i}$, $i = 1, ..., d$. As a result, one obtains a decomposition of the trajectory matrix into a sum of matrices $\mathbf{X} = \sum_{i=1}^{d} \mathbf{E}_i$, where $\mathbf{E}_i = \sqrt{\lambda_i}\mathbf{U}_i\mathbf{V}_i^T$.

Step 3 (Reconstruction)**:** Each elementary matrix $\mathbf{E}_k(z_{ij}) \in \Re^{L_0 \times K}$ is then transformed into a principal component of length N_0, named g_k , $k = 1, ..., d$, as in (6) which applies a linear transformation known as diagonal averaging or Hankelization.

$$g_k = \begin{cases} (1/(k+1)) \sum_{m=1}^{k+1} z_{m,k-m+2}, & 0 \le k < L* - 1, \\ (1/L*) \sum_{m=1}^{L*} z_{m,k-m+2}, & L* - 1 \le k < K*, \\ (1/(N_0-k)) \sum_{m=k-K*+2}^{N_0-K*+1} z_{m,k-m+2}, & K* \le k < N_0, \end{cases} \tag{6}$$

where $L* = \min(L_0, K)$, $K* = \max(L_0, K)$.

3. PROCESSING MEASUREMENT DATA AND CONSTRUCTING A MULTI-FEATURE

Let consider a measurement data set as in (7):

$$\bar{\mathbf{X}} = [\bar{\mathbf{X}}_1, ..., \bar{\mathbf{X}}_{n_0}] \in \Re^{N \times n_0}, \tag{7}$$

where $\bar{\mathbf{X}}_i = [x_{1i}, x_{2i}, ..., x_{Ni}]^T$, $i = 1, ..., n_0$, is called the data vector of the i-th state variable. n_0 is the number of state variables, or the number of the physical parameters to be employed to build the data set, such as the mechanical vibration acceleration, displacement, frequency, etc; in the surveys in Section 5, the only acceleration signal is exploited, so $n_0 = 1$.

3.1. Filtering noise based on SSA

The method of filtering high-frequency noise presented in [8, 22] is adopted here to process the data set (7). For each column $\bar{X}_i$, by using SSA we obtain Q_{SSA}time series with different frequencies. Due to the trend of the mechanical vibration components concentrates most of their power on the low-frequency ranges, among these series

we retain only Q ones corresponding to the lowest frequency ranges; the others owning the high frequencies are considered as noise. A new data set ${}_i\mathbf{G}$ obtained by this way is shown as in (8), in which the length of each vector ${}_i\mathbf{g}^{(h)}$, $h = 1, ..., Q$, is N.

$$ {}_i\mathbf{G} = \{{}_i\mathbf{g}^{(1)}, ..., {}_i\mathbf{g}^{(Q)}\}, \;\; i = 1...n_0. \tag{8} $$

3.2. Building a multi-feature for damage identification

3.2.1 Formulation

Let consider the h-th series ${}_i\mathbf{g}^{(h)}$ of ${}_iG(8)$

$$ {}_i\mathbf{g}^{(h)T} = ({}_i\bar{z}_1^{(h)}, {}_i\bar{z}_2^{(h)}, ..., {}_i\bar{z}_N^{(h)}), \;\; h = 1...Q. \tag{9} $$

By selecting two adaptive indexes to be the step (st) and window length (L_0), we construct a new matrix ${}_i\mathbf{X}_h \in \Re^{(L_0+st)\times P_0}$ deriving from ${}_i\mathbf{g}^{(h)}$ as below:

$$ {}_i\mathbf{X}_h = \begin{pmatrix} {}_i\bar{z}_1^{(h)} & {}_i\bar{z}_{st+1}^{(h)} & \cdots & \cdots & {}_i\bar{z}_{(P_0-1)st+1}^{(h)} \\ \vdots & \vdots & \cdots & \cdots & \vdots \\ {}_i\bar{z}_{st}^{(h)} & {}_i\bar{z}_{2st}^{(h)} & \ddots & \iddots & {}_i\bar{z}_{P_0st}^{(h)} \\ \vdots & \vdots & \iddots & \ddots & \vdots \\ {}_i\bar{z}_{L_0+st}^{(h)} & {}_i\bar{z}_{L_0+2st}^{(h)} & \cdots & \cdots & {}_i\bar{z}_{L_0+P_0st}^{(h)} \end{pmatrix}, $$

or in another form as in (10):

$$ {}_i\mathbf{X}_h = \begin{pmatrix} Z_{11} & \cdots & Z_{1j} & \cdots & Z_{1P_0} \\ \vdots & \ddots & \vdots & \iddots & \vdots \\ Z_{k1} & \cdots & Z_{kj} & \cdots & Z_{kP_0} \\ \vdots & \iddots & \vdots & \ddots & \vdots \\ Z_{(L_0+st)1} & \cdots & Z_{(L_0+st)j} & \cdots & Z_{(L_0+st)P_0} \end{pmatrix}. \tag{10} $$

We then create a column vector of P_0elements ${}_i\mathbf{a}_{me}^{(h)} = [{}_ia_{me(1)}^{(h)}, ..., {}_ia_{me(P_0)}^{(h)}]^T$. The j-th one is constituted of the elements in the j-th column of ${}_i\mathbf{X}_h$ as follows:

$$ {}_ia_{me(j)}^{(h)} = K_{me}\frac{1}{L_0+st}\sum_{k=1}^{L_0+st}|Z_{kj}|; \;\; h=1...Q, \;\; j=1...P_0. \tag{11} $$

Above, $K_{me} > 0$ is a default parameter selected by the designer to adjust the amplitude.

Remark 1: It should be noted that ${}_ia_{me(j)}^{(h)}$, $i = 1, ..., n_0$, $h = 1, ..., Q$, $j = 1, ..., P_0$, in (11) derives from the i-th physical parameter (or the i-th state variable) in (7), hence it is the mean-quantification in the j-th sampling duration of the signal belonging to the h-th frequency range (or the h-th principal component of SSA) of this physical parameter.

We then define vector ${}_i\mathbf{a}_{me}^{(h)} = [{}_i\mathrm{a}_{me(1)}^{(h)}, ..., {}_i\mathrm{a}_{me(P_0)}^{(h)}]^T$ to depict the h-th single-feature corresponding to the h-th principal component of SSA belonging to the i-th state variable. Due to $i = 1, ..., n_0$ and $h = 1, ..., Q$, so from these vectors we obtain matrix $\mathbf{M}_f \in \Re^{P_0\times(n_0Q)}$ below:

$$ \mathbf{M_f} = [{}_1\mathbf{a}_{me}^{(1)}, ..., {}_1\mathbf{a}_{me}^{(Q)} \cdots {}_{n_0}\mathbf{a}_{me}^{(1)}, ..., {}_{n_0}\mathbf{a}_{me}^{(Q)}] \in \Re^{(P_0\times n_0Q)}, \tag{12a} $$

$$ \underset{(P_0\times n_0Q)}{\mathbf{M_f}} = \begin{pmatrix} {}_1\mathrm{a}_{me(1)}^{(1)} & \cdots & {}_1\mathrm{a}_{me(1)}^{(Q)} & {}_{n_0}\mathrm{a}_{me(1)}^{(1)} & \cdots & {}_{n_0}\mathrm{a}_{me(1)}^{(Q)} \\ \vdots & & \vdots & \vdots & & \vdots \\ {}_1\mathrm{a}_{me(k)}^{(1)} & \ddots & {}_1\mathrm{a}_{me(k)}^{(Q)} & {}_{n_0}\mathrm{a}_{me(k)}^{(1)} & \ddots & {}_{n_0}\mathrm{a}_{me(k)}^{(Q)} \\ \vdots & & \vdots & \vdots & & \vdots \\ {}_1\mathrm{a}_{me(P_0)}^{(1)} & \cdots & {}_1\mathrm{a}_{me(P_0)}^{(Q)} & {}_{n_0}\mathrm{a}_{me(P_0)}^{(1)} & \cdots & {}_{n_0}\mathrm{a}_{me(P_0)}^{(Q)} \end{pmatrix}. \tag{12b} $$

Each row of $\mathbf{M_f}$ in the form of a row vector signed $\mathbf{f}$ $(1 \times n_0Q)$ constitutes a multi-feature. At the k-th sampling time duration, $k = 1, ..., P_0$, the multi-feature is quantified as in (13), where ${}_i\mathrm{a}_{me(k)}^{(j)}$ comes from (11).

$$ \mathbf{f}_{(k)} = \left[{}_1\mathrm{a}_{me(k)}^{(1)} \cdots {}_1\mathrm{a}_{me(k)}^{(Q)} \cdots {}_{n_0}\mathrm{a}_{me(k)}^{(1)} \cdots {}_{n_0}\mathrm{a}_{me(k)}^{(Q)}\right]_{(1\times n_0Q)}, \;\; k = 1...P_0. \tag{13} $$

The multi-feature reflects the dynamic response characteristics of the mechanical system at each sampled time duration. It collects local information of the mechanical-system dynamic response. Each element ${}_i\mathrm{a}_{me(k)}^{(j)}$ (11) of $\mathbf{f}_{(.)}$(13) is so-called SSA-based data's local feature coefficient (SS-DLFC). To enhance the capability of the multi-feature to distill valuable information from the database, optimizing parameters (st, Q, L_0, P_0) in (11) is carried out as in Section 4.

3.2.2 Attributes of the SS-DLFC and the multi-feature

We perform a short survey to analyze and evaluate the functional attributes of the SS-DLFC and the multi-feature. Some bearing-fault data sets measured by acceleration sensors in the experimental apparatus detailed in Section 5 are used. Due to following the acceleration sensors only, the number of state variables in this case is $n_0 = 1$ (see (7)). Fig. 1 shows $a_{me(i)}^{(2)}$, $i = 1...P_0$, deriving from $L_0 = 8000$, $st = 200$, $P_0 = 300$, Q=20, and $K_{me} = 30$ and the second principal component of SSA in 10 different damage statuses of the bearing. They related to the bearing undamaged or being damaged at the inner or outer or ball with the damage levels 1 to 3, under the 2-typed load. For example, 'Damage1-Ball' denoted the bearing was damaged level 1 at the ball, the 2-typed load.

It should be noted that 1) the bearing status was almost not changed during each of the surveyed time durations to

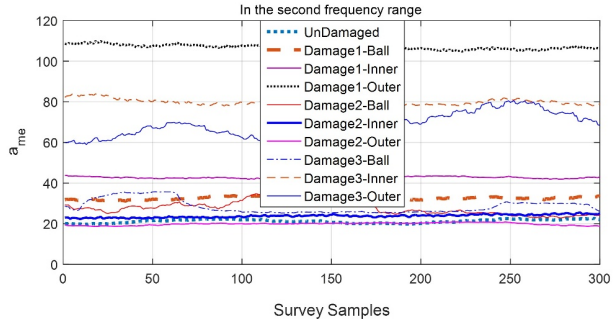

Fig. 1. Value of the SS-DLFC in ten statuses of the surveyed bearing.

build the corresponding line in Fig. 1, and 2) the ten lines in the figure express the ten different statuses of the bearing. It is possible to draw from Fig. 1 that the SS-DLFC and the proposed multi-feature **f** satisfy two functional attributes as below.

1) Stability attribute: The stability attribute of a feature requires that if there is not any considerable change in the system damage status, then the varying range of the feature must be narrow. Conversely, if the system fault varying tendency is upholden then the corresponding varying trend of the feature must be changed more quickly and conserved stably.

This attribute of the SS-DLFC can be recognized clearly in the figure via the two following characteristics: a) each line to be located in a corresponding narrow area, and b) the ten lines to be quite individual.

2) Dispersion attribute: It expresses the sensibility of a feature. Related to a graph, the dispersion attribute here displays the capability to distinguish clearly the difference between the lines depicting the feature corresponding to different damage statuses.

The dispersion attribute of the SS-DLFC can be implied from Fig. 1 via the different fault cases (damage degree and/or area) such as the Undamaged, Damage1-Outer, Damage1-Ball, Damage3-Outer, etc.

Because the proposed multi-feature **f** is constituted of the SS-DLFC coming from Q the independent frequency ranges of the original signal, so its attributes coincide with that of the SS-DLFC as abovementioned.

Remark 2: From the stability and dispersion attributes, it can infer that if system mechanical status is sustained, there will exist a narrow varying area established by the SS-DLFC corresponding to each status. This can be seen as the manifestation reflecting the system fault status.

Remark 3: In Fig. 1, despite deriving from the different damage cases, there sometimes exist overlapped ranges from some lines. So, to exploit the SS-DLFC effectively we use the multi-feature **f** instead of the single one, SS-DLFC, and adopt an ANFIS with an unsupervised learning process; the ANFIS can interpolate the real status of the surveyed object via the multi-feature as presented in the algorithm AfOBSM.

Remark 4: The SS-DLFC (11) follows the mean-value idea presented in [34–39]. However, it exploits an adaptive window depicted by (L_0, st) which will be optimized when operating the proposed algorithm (see (16) in Section 4). Thus, SS-DLFC can maintain the local property of data when taking the dual function as mention in Section 1: distilling the valuable information in data and filtering low-frequency noise along with blurring the negative effects of IN as well as of external disturbance.

4. PROPOSED ALGORITHM FOR OBSM

4.1. Building database

As presented in Section 3, for the d-th fault kind ($d = 1, ..., D$), we obtain $\mathbf{M_f}$ (12). It is now re-signed ${}^d\mathbf{M_f}$ to denote the d-th fault kind. Using this way for D the considered bearing's typical fault kinds, we obtain data matrix $\mathbf{W} \in \Re^{(P\times n)}$ as in (14).

$$\mathbf{W} = [\ {}^1\mathbf{M_f} \quad {}^d\mathbf{M_f} \quad {}^D\mathbf{M_f}\ ]^T \in \Re^{(P\times n)},$$
$$P = DP_0, \quad n = Qn_0. \tag{14a}$$

Corresponding to the input data space **W**, we then encode D the bearing's typical fault kinds as below:

$$\mathbf{y} = [y_{11}, ..., y_{1P_0}, ..., y_{D1}, ..., y_{DP_0}]^T$$
$$\equiv [y_1, ..., y_P]^T \in \Re^{P\times 1}. \tag{14b}$$

Finally, a database called the historical data set or the initial data space (IDS) for training ANFIS is created as in (15), where $\mathbf{W}_{tr} \equiv \mathbf{W}$ comes from (14).

$$\text{IDS} = \langle input - output \rangle \equiv \langle \mathbf{W}_{tr} - \mathbf{y} \rangle. \tag{15}$$

Remark 5: From Remark 4, the SS-DLFC (11) can filter low-frequency noise and blur the negative effects of IN as well as of external disturbance. So, the role of the combination of SSA-based high-frequency filtering and (11)-based filtering can be seen as an integrated filtering system (INFS). The AfOBSM is therefore depicted via the INFS as in its flowchart in Fig. 2.

4.2. Algorithm AfOBSM

There are two phases as in Fig. 2. The offline is to identify the dynamic response of the mechanical system where the bearing is fixed. Firstly, by initializing the parameters (Q, st, L_0, P_0) in (11), the IDS (15) is built. By using the same way of building $\mathbf{W}_{tr}$ we also set up a test set $\mathbf{W}_{te}$ whose structure and size are similar to that of $\mathbf{W}_{tr}$. An ANFIS is trained upon the IDS and the algorithm FIN-ANFIS [24]. A loop process is then operated upon the algorithm DE [40] to optimize (Q, st, L_0, P_0). In this process, $\mathbf{W}_{te}$ is employed to adjust the parameters after each loop l until either their optimal values to be determined or $l > [l]$. As

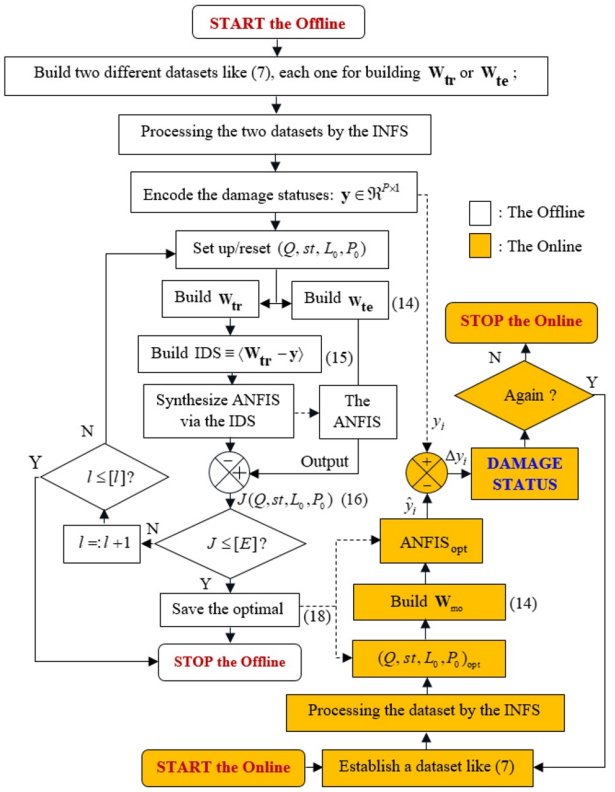

Fig. 2. Flowchart of the AfOBSM.

a result, we obtain an optimal ANFIS signed ANFIS$_{opt}$, and the optimal parameters $(Q, st, L_0, P_0)_{\text{opt}}$for the online phase.

The online phase undertakes the OBSM during the mechanical system operating process upon the interpolating ability of the ANFIS$_{\text{opt}}$. At checking time, the vibration measurement is performed online to build an input data set signed $\mathbf{W}_{\text{mo}}$ using $(Q, st, L_0, P_0)_{\text{opt}}$ such that it is similar to the form and size of the matrix (12), $\mathbf{W}_{\text{mo}} \equiv \mathbf{M}_f \in \Re^{P_0 \times (n_0 Q)}$. By using $\mathbf{W}_{\text{mo}}$ as the input of the ANFIS$_{opt}$, $\Delta y_i = y_i - \hat{y}_i$ will reflect the status of the bearing(s) as presented in Step 5 of the AfOBSM. Where, y_i and $\hat{y}_i$ respectively are the i-th data output and the correspoinding output of the ANFIS$_{\text{opt}}$.

Algorithm AfOBSM

In the offline phase: Identify the dynamic response of the mechanical system fixed the bearing(s).
Initialize the parameters in (11) to be (Q, st, L_0, P_0).
Step 1: Build $\mathbf{W}_{\text{tr}}$, $\mathbf{W}_{\text{te}}$ (14a)) and set up the IDS (15).
Step 2: Identify the system by an ANFIS based on the IDS and the algorithm FIN-ANFIS [24].
Step 3: Optimize (Q, st, L_0, P_0).
Use $\mathbf{W}_{\text{te}}$ as the input of the ANFIS and estimate the objective function J (16).

$$J(Q, st, L_0, P_0) \equiv = E = \sqrt{P^{-1} \sum_{i=1}^{P} (\Delta y_i)^2} \to [E], \quad (16)$$

$$\Delta y_i = y_i - \hat{y}_i. \quad (17)$$

If (16) not converge: call the DE [40] to adjust (Q, s, L_0, P_0) and return to Step 1; otherwise, save the optimal ones as in (18), and stop the offline.

$$[\text{ANFIS}_{\text{opt}}, (Q, st, L_0, P_0)_{\text{opt}}]. \quad (18)$$

In the online phase: Recognize the bearing(s) status.
Step 4: Build $\mathbf{W}_{\text{mo}}$.
Step 5: Conclusion
By utilizing $\mathbf{W}_{\text{mo}}$ as the input of the ANFISopt in (18), the present status of the bearing(s) can be recognized, which is the q-th one encoded in $\mathbf{y}$ (15) such that

$$\sum_{j=1}^{P_0} |\Delta y_{qj}| = \min_k \sum_{j=1}^{P_0} |\Delta y_{kj}|, \quad k = 1, ..., D.$$

Remark 6: 1) To enhance the effectiveness, $\mathbf{W}_{\text{tr}}$ should cover almost the typical fault kinds of a bearing; and the datasets for building $\mathbf{W}_{\text{tr}}$ and $\mathbf{W}_{\text{te}}$ must be measured at two separate times. 2) In the offline, the role of the ANFIS$_{\text{opt}}$ is to identify the dynamic response of the mechanical system via $\mathbf{W}_{\text{tr}}$. Meanwhile, in the online, the ANFIS$_{\text{opt}}$ can interpolate all behaviors of the system via $\mathbf{W}_{\text{mo}}$, even if the ones not being trained.

5. EVALUATING THE PROPOSED METHOD

5.1. Experimental apparatus and approach way

The experimental apparatus in Fig. 3 is used to verify the proposed method. In the apparatus, (1) and (3) are the checked bearings; (2) and (4) are acceleration sensors; (5) is a computer for installing the relative software and connecting with the hardware, (6) is the module for processing and transforming time-series vibration signal (Model: NI-9234). Besides, a disc brake was also installed in the system to adjust load impacting on the bearings. We consider bearing (3) under different load levels via the signal from sensor (2) and sensor (4).

We used the laser cutting technology to create the fault types on the bearings as in Table 1 with some notations as follows. The damaged location at the Inner or Outer or Balls respectively is signed In, Ou, or Ba. Four considered damage degrees are undamaged or damaged with degrees from 1 to 3 which are signed UnD, D1, D2, and D3, respectively. Three load levels are signed by L1, L2, or L3. The above notations are used to abbreviate the surveyed cases. For example, L_mD_nBa expresses the bearing under the load m (1, ..., 3), to be damaged level n (1, ..., 3) at the ball.

We utilize four measuring datasets as follows. The first one (signed FtDS) is 121,000-sample set constituted of L_1UnD, L_1D_1In, L_1D_2In, L_1D_3In, L_1D_1Ou, L_1D_2Ou, and L_1D_3Ou. The second one (signed SDS) is 121,000-sample

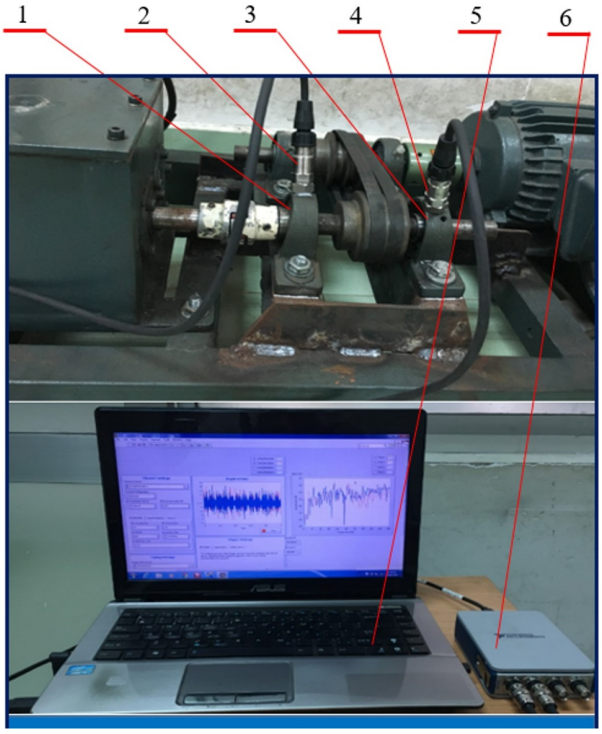

Fig. 3. Experimental apparatus.

Table 1. The fault types to be made in the bearing (3).

Fault bearing cases	Crack size	
Fault degrees (1-3) and their location	Width (mm)	Depth (mm)
D1Ou	0.20	0.3
D2Ou	0.30	0.3
D3Ou	0.46	0.3
D1In	0.20	0.3
D2In	0.30	0.3
D3In	0.40	0.3
D1Ba	0.15	0.2
D2Ba	0.20	0.2
D3Ba	0.25	0.2

set from L_2UnD, L_2D_1In, L_2D_2In, L_2D_3In, L_2D_1Ba, L_2D_2Ba, and L_2D_3Ba. The third one (signed TDS) is 121,000-sample set from L_3UnD, L_3D_1Ou, L_3D_2Ou, L_3D_3Ou, L_3D_1Ba, L_3D_2Ba, and L_3D_3Ba. While the fourth one (signed FhDS) is 175,000-sample set deriving from L_2UnD, L_2D_1In, L_2D_2In, L_2D_3In, L_2D_1Ou, L_2D_2Ou, L_2D_3Ou, L_2D_1Ba, L_2D_2Ba, and L_2D_3Ba.

To compare, together with the proposed AfOBSM, the intelligent fault diagnosis relied on unsupervised learning towards mechanical big data [7], the bearing fault diagnosis method using ANFIS, SSA, sparse filtering and big data [8], and the method of damage-diagnosis based on ANFIS and wavelet analysis [19] are used to identify fault status of the bearing (3) in Fig. 3 in two cases. The first case relies on the signal from the nearby sensor (4) while the other uses the farther sensor (2).

The RMSE E (19) and the percentage accuracy Ac (20) are used, where Δy_i is the error shown in Fig. 2; P is the number of the surveyed samples; $cr\_samples$ denotes the number of samples expressing correctly the real status of the bearing (among the P samples).

$$E = \left(\sum_{i=1}^{P} (\Delta y_i)^2 / P\right)^{0.5}. \tag{19}$$

$$\text{Ac} = 100 \times cr\_samples/P \ \ (\%). \tag{20}$$

Also, we use the mean value (MV) of Ac in each survey. Let D be the number of fault types existing in the database for the survey, Ac_d, $d = 1...D$, be Ac (20) corresponding to the d-th fault type, then

$$\text{MV} = \sum_{d=1}^{D} \text{Ac}_d / D(\%). \tag{21}$$

5.2. Survey of AfOBSM's functional parameters

5.2.1 Series length N

The optimal results $(Q, st, L_0, P_0)_{\text{opt}}$in (18) depends deeply on the sought area reflected by the time-series length N in (7). Therefore, quantifying an appropriate value of N for each application to reduce the calculating cost needs to be performed. For this, we performed surveys via the FtDS to obtain the results as in Fig. 4 and Table 2. As in Fig. 4(a), with increasing N from 60,000 to 70,000, the E (19) of the ANFIS reduces considerably. In its larger varying range as in Fig. 4(b), when $N < 50,000$, the increase of N makes Ac (%) go up quickly; this tendency is not maintained when $N > 70,000$; while in case $N > 100,000$, Ac and the ANFIS's training time t_{ANFIS} are quite stable, but the time duration $t_{\text{F}_{\text{mo}}}$ for building $\mathbf{W}_{\text{mo}}$ grows up quickly. This is a disadvantage for the online phase of the AfOBSM. Therefore, we will use $N = 100,000$ for the FtDS-based surveys. By the similar way, we also speculated the other databases. As a result, the fit values of N related to SDS and TDS are 100,000, while N related to FhDS is 150,000.

5.2.2 Length P_0

In fact, it is difficult to estimate P_0 via theoretical analyzation. In this study, we carry out a loop process in the offline phase to adjust P_0 together with (Q, st, L_0) until $J(Q, st, L_0, P_0) \equiv E \to [E]$ (16) as in Fig. 2. Table 3 shows some extractions from the obtained results where the ANFIS was used to approximate the FtDS ($\mathbf{W}_{\text{tr}} \in \Re^{(121,000\times 7)}$) with $[E] = 10^{-5}$. The table shows that ANFIS training time t_{ANFIS} increases quickly when P_0 goes up. Also, E reaches to $[E]$ when $P_0 \to 2,500$. To weaken the calculating cost, we therefore selected two values of P_0 which were 2,500 for the set FhDS and 3,000 for the other data sets FtDS, SDS, TDS.

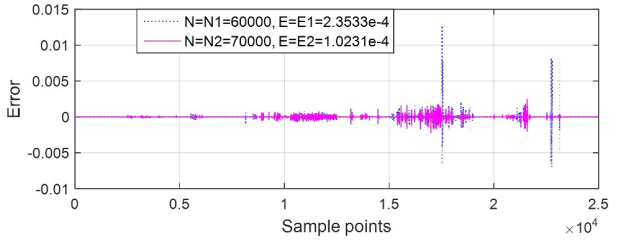

(a)

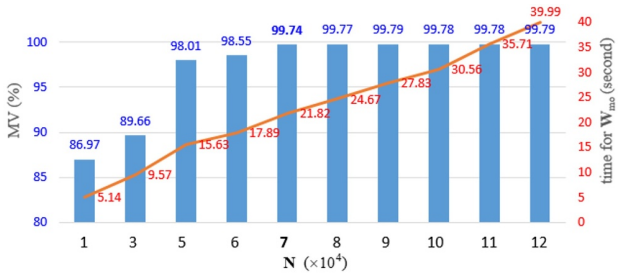

(b)

Fig. 4. Influence of N: the error $\Delta y_i = y_i - \hat{y}_i$ (see Fig. 2) in two cases, $N = 60,000$ and $N = 70,000$ (a)the relation between N and (signed 'time for $\mathbf{W}_{mo}$' in the figure), as well as MV of the AfOBSM (b).

Table 2. The influence of N on $t_{F_{mo}}$ when building $\mathbf{W}_{mo}$, time for training the ANFIS in the offline phase t_{ANFIS} and the accuracy Ac of the proposed method.

N ($\times 10^4$)	$t_{F_{mo}}$ (second)	t_{ANFIS} (minute)	Ac (%)
1	5.14	67.76	86.97
2	7.07	66.05	88.18
3	9.57	66.19	89.66
4	12.98	63.44	96.54
5	15.63	66.71	98.01
6	17.89	66.34	98.55
7	21.82	67.24	99.74
8	24.67	68.56	99.77
9	27.83	67.45	99.79
10	30.56	68.82	99.78
11	35.71	69.94	99.78
12	39.99	69.01	99.79

5.2.3 Length of the step *st*

The set FtDS having 121,000 data samples together with $P_0 = 2,500$, $L_0 = 8,000$, $N = 100,000$, $Q = 7$ were used to survey the relationship between the step st and the stability ability of the single feature $a^{(.)}_{me(.)}$ (11). The obtained results showed that an appropriate value of st influenced positively on the effectiveness of the proposed method. However, the stability of the single feature could be maintained in a quite widely varying range of the step st. As in Fig. 5, the single feature is maintained stably in a narrow range during the varying process of st in [180, 220], even if it was calculated from two different time series $\mathbf{W}_{tr}$ and $\mathbf{W}_{mo}$. This is really meaningful to reduce the training time related to specifying the optimal parameters $(Q, st, L_0, P_0)_{opt}$. From this result, $st = 200$ will be employed for all our surveys in the rest of this section.

Table 3. The relation between E, t_{ANFIS} (minute) and P_0.

P_0	2200	2500	2800	3000	3200
t_{ANFIS}	65.89	76.87	89.56	104.2	125.1
E ($\times 10^{-4}$)	2.199	0.391	0.381	0.378	0.370

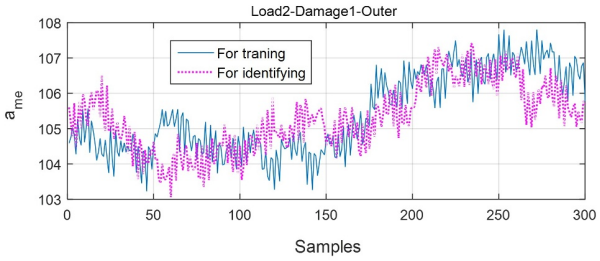

Fig. 5. The single feature deriving from $\mathbf{W}_{tr}$ when $st = 180$ (signed 'For training') or deriving from $\mathbf{Q}_{mo}$ when $st = 220$ (signed 'For identifying'), in which $\mathbf{W}_{tr}$ and $\mathbf{W}_{mo}$ came from a similar bearing status (L_2D_1Ou).

Table 4. Ac (%) of the methods corresponding to the data set FhDS from sensor 2 (see Fig. 3).

Data	[7]	[8]	[19]	Proposed
L_3UnD	98.13	98.25	91.34	98.34
L_3D_1In	96.34	97.11	94.87	97.24
L_3D_2In	95.53	95.08	95.23	99.94
L_3D_3In	97.14	95.94	93.44	99.65
L_3D_1Ou	93.57	97.16	92.45	96.76
L_3D_2Ou	97.59	97.93	96.11	99.12
L_3D_3Ou	96.98	97.64	90.89	96.75
L_3D_1Ba	94.09	96.53	92.77	98.97
L_3D_2Ba	98.34	98.77	95.20	98.21
L_3D_3Ba	95.50	95.85	90.99	98.90

5.3. Comparison results

The AfOBSM along with the other methods were adopted to recognize fault status of the bearing (3) via different datasets consisting of the FtDS, SDS, TDS, and the FhDS measured from either sensor (2) or sensor (4) as in Fig. 3. The obtained results were shown in Figs. 6-9 and Tables 4-5.

Generally, the prediction outputs of the proposed method track quite well the real fault statuses of the

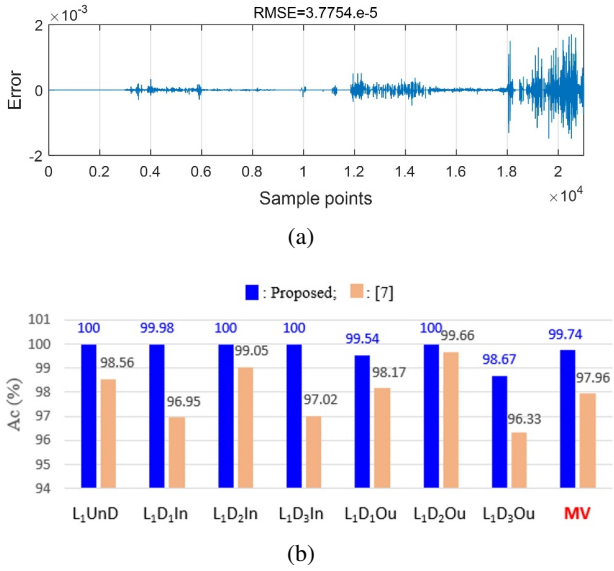

Fig. 6. Surveying via the data set FtDS: the error Δy_i and the RMSE of the AfOBSM (a); Ac (20) and MV (21) of the AfOBSM and [7] (b).

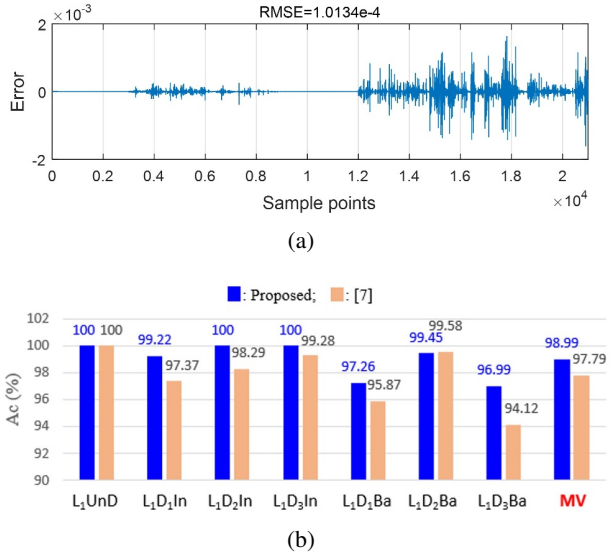

Fig. 7. Deriving from the SDS: Δy_i and the RMSE of the AfOBSM (a); Ac and MV of the AfOBSM and [7] (b).

Table 5. MV (%) of the methods corresponding to each dataset (S2: sensor 2; S4: Sensor 4).

Data	[7]	[8]	[19]	Proposed
FtDS	97.96	98.19	91.45	99.74
SDS	97.79	97.93	89.98	98.99
TDS	97.29	98.14	93.67	99.40
FhDS (S2)	96.32	97.03	93.33	98.55
FhDS (S4)	97.81	96.05	94.08	97.99

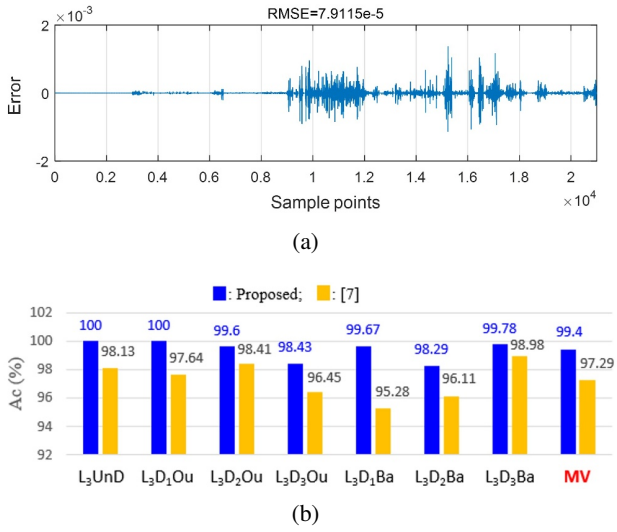

Fig. 8. Deriving from the TDS: Δy_i and the RMSE of the AfOBSM (a); Ac and MV of the AfOBSM and [7] (b).

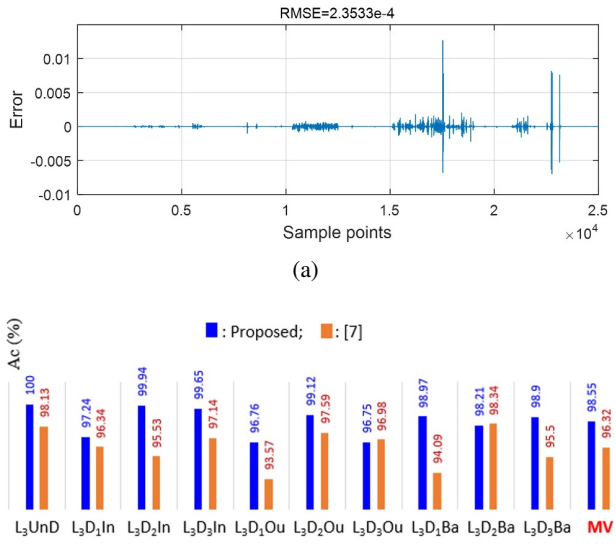

Fig. 9. Deriving from the SDS: Δy_i and the RMSE of the AfOBSM (a); Ac and MV of the AfOBSM and [7] (b).

bearing. For example, MV in Figs. 6-9 respectively are 99.74, 98.99, 99.40, and 98.55%. The prediction outputs of the ANFIS$_{opt}$ created by the AfOBSM as illustrated in Fig. 2 can reach well the corresponding encoded values expressed by $\Delta y_i = y_i - \hat{y}_i$. This is expressed by the very small RMSEs of Δy_i given in Figs. 6-9 respectively to be $3.7754.10^{-5}$, $1.0134.10^{-4}$, $7.9115.10^{-5}$, and $2.3533.10^{-4}$. The comparing results from them also show that among the four considered methods, the AfOBSM is

the best. For example, from Table 5 corresponding to the dataset FhDS (sensor 4), MV (%) of [7], [8], [19], and the proposed respectively are 97.81, 96.05, 94.08, and 97.99.

Finally, based on MV of these methods using the dataset FhDS measured from either the nearby sensor (4) or the farther sensor (2) in Table 5, it can infer that signal from both sensors can be employed effectively. There is not any common tendency to be recognized from the last two rows in Table 5. It means, similar to the others, the proposed method is not too sensitive to the sensor-installing location. This characteristic enhances the reliability and feasibility of the method to deal with more complex mechanical systems.

6. CONCLUSION

The new method for OBSM has been presented via the proposed algorithm AfOBSM. The sensitive and stable multi-feature constituted of the single features SS-DLFCs was discovered to better the ability to distill valuable information in massive and noisy data. Theoretical analysis showed that together with taking the main role of describing the mechanical dynamic response, the multi-feature could also blur the negative effect of impulse noise and external disturbance, and keep the local characteristics of data. To accommodate online large database processing in the wide frequency ranges including IN, the mechanism of the combination of the SSA based filtering and SS-DLFC based filtering was presented. These aspects were incorporated to constitute the AfOBSM. Surveys based on the experimental-system were performed. The obtained results showed that the system of OBSM built by the AfOBSM could track the bearing real fault statuses with an accuracy higher than that from the considered others. Also, the OBSM system was not too sensitive to sensor-installing locations. It is a necessary characteristic to ensure reliability and feasibility when dealing with more complex systems.

Despite focusing on the online approach, the dynamic attributes of the evolving data streams (EDSs) coming from the sensors, however, did not be considered when building the databases for the AfOBSM. This impacts negatively on the effectiveness of the proposed method. How to deal with EDSs to improve the method of OBSM will be paid attention to in our next research.

REFERENCES

[1] X. Yin and S. Lafortune, "On the decidability and complexity of diagnosability for labeled Petri nets," *IEEE Trans. on Auto. Control*, vol. 62, no. 11, pp. 5931-5938, 2017.

[2] X. Yin, J. Chen, Z. Li, and S. Li, "Codiagnosability analysis of bounded Petri nets," *IEEE Trans. on Auto. Control*, vol. 63, no. 4, pp. 1192-1199, 2018.

[3] X. Yin, J. Chen, Z. Li, and S. Li, "Robust fault diagnosis of stochastic discrete event systems," *IEEE Trans. on Auto. Control*, vol. 64, no. 10, pp. 4237-4244, 2019.

[4] L. Liu, Y.J. Liu, and S. Tong, "Neural networks-based adaptive finite-time fault-tolerant control for a class of strict-feedback switched nonlinear systems," *IEEE Trans. on Cyb.*, vol. 49, no. 7, pp. 2536-2545, 2019.

[5] X. Xie, D. Yue, and J. H. Park, "Observer-based fault estimation for discrete-time nonlinear systems and its application: A weighted switching approach," *IEEE Transactions on Circuits and Systems - I: Regular Papers*, vol. 66, no. 11, pp. 4377-4387, 2019.

[6] T. Boukra, "Identifying new prognostic features for remaining useful life prediction using particle filtering and neuro-fuzzy system predictor," *Proc. of IEEE 15th Inter. Conf. on Envir. and Elect. Eng.*, Rome, Italy, 2015.

[7] L. Yaguo, J. Feng, L. Jing, X. Saibo, and X. D. Steven, "An intelligent fault diagnosis method using unsupervised feature learning towards mechanical big data," *IEEE Trans. on Ind. Electro.*, vol. 63, no. 5, pp. 3137-3147, 2016.

[8] Q. T. Tran, S. D. Nguyen, and T. I. Seo, "Algorithm for estimating online bearing fault upon the ability to extract meaningful information from big data of intelligent structures," *IEEE Trans on Industrial Electro.*, vol. 66, no. 5, pp. 3804-3813, 2019.

[9] V. S. Jigajinni and V. Upendranath, "ANFIS-based fault diagnosis tool for a typical small aircraft fuel system," *Proc. of Inter. Conf. on Intelli. Comm., Control and Devices. Advances in Intelli. Systems and Computing*, Springer, Singapore, pp. 391-405, 2017.

[10] A. K. Mahamad and T. Hiyama, "Fault classification based artificial intelligent methods of induction motor bearing," *Int. J. Innov. Comput., Inf. Control*, vol. 7, no. 9, pp. 5477-5494, 2011.

[11] Z. Tong, W. Li, B. Zhang, F. Jiang, and G. Zhou, "Online bearing fault diagnosis based on a novel multiple data streams transmission scheme," *IEEE Access*, vol. 7, pp. 66644-66654, 2019.

[12] J. Chebil, M. Hrairi, and N. Abushikhah, "Signal analysis of vibration measurements for condition monitoring of bearings," *Australian J. Basic Appl. Sci.*, vol. 5, no. 1, pp. 70-78, 2011.

[13] S. D. Wu, C. W. Wu, T. Y. Wu, and C. C. Wang, "Multi-scale analysis based ball bearing defect diagnostics using Mahalanobis distance and support vector machine," *Entropy*, vol. 15, no. 2, pp. 416-433, 2013.

[14] J. F. Zhang and Z. C. Huang, "Kernel Fisher discriminant analysis for bearing fault diagnosis," *Proc. of Inter. IEEE Conf. on Machine Learning and Cybernetics*, Guangzhou, China, pp. 3216-3220, 2005.

[15] W. Sun, G. Yang, Q. Chen, A. Palazoglu, and K. Feng, "Fault diagnosis of rolling bearing based on wavelet transform and envelope spectrum correlation," *J. Vib. and Control*, vol. 19, no. 6, pp. 924-941, 2013.

[16] B. Sreejith, A. Verma, and A. Srividya, "Fault diagnosis of rolling element bearing using time-domain features and neural networks," *Proc. of The 3rd Inter. IEEE Conf. on Ind. and Infor. Sys.*, India, 2008.

[17] W. Q. Wang, M. F. Golnaraghi, and F. Ismail, "Prognosis of machine health condition using neuro-fuzzy systems," *Mech. Sys. and Sig. Pro.*, vol. 18, pp. 813-831, 2004.

[18] I. K. Jeong, M. Kang, J. Kim, J. M. Kim, J. M. Ha, and B. K. Choi, "Enhanced DET-based fault signature analysis for reliable diagnosis of single and multiple-combined bearing defects," *Shock and Vibration*, Article ID 814650, 10 pages, 2016.

[19] S. D. Nguyen, K. N. Ngo, Q. T. Tran, and S. B. Choi, "A new method for beam-damage-diagnosis using adaptive fuzzy neural structure and wavelet analysis," *Mech. Sys. and Signal Pro.*, vol. 39, pp. 181-194, 2013.

[20] D. R. Salgado and F. J. Alonso, "Tool wear detection in turning operations using singular spectrum analysis," *J. of Mate. Proc. Tech.*, vol. 171, pp. 451-458, 2006.

[21] B. Kilundu, P. Dehombreux, and X. Chiementin, "Tool wear monitoring by machine learning techniques and singular spectrum analysis," *Mech. Sys. and Sig. Proc.*, vol. 25, pp. 400-415, 2011.

[22] N. Golyandina and Z. Nekrutkin, *Analysis of Time Series Structure - SSA and Related Techniques*, Chapman & Hall/CRC, Boca Raton, Florida, 2001.

[23] T. Liu, J. Chen, and G. Dong, "Singular spectrum analysis and continuous hidden Markov model for rolling element bearing fault diagnosis," *J. of Vib. and Control*, vol. 21, no. 8, pp. 1506-1521, 2015.

[24] S. D. Nguyen, S. B. Choi, and T. I. Seo, "Recurrent mechanism and impulse noise filter for establishing ANFIS," *IEEE Trans. on Fuzzy Systems*, vol. 26, no. 2, pp. 985-997, 2018.

[25] S. D. Nguyen, Q. H. Nguyen, and T. I. Seo, "ANFIS deriving from jointed input-output data space and applying in smart-damper identification," *Applied Soft Computing*, vol 53, pp. 45-60, 2017.

[26] S. D. Nguyen and T. I. Seo, "Establishing ANFIS and the use for predicting sliding control of active railway suspension systems subjected to uncertainties and disturbances," *Inter. J. of Mach. Learning and Cybernetics*, vol. 9, pp. 853-865, 2018.

[27] S. D. Nguyen, H. D. Vo, and T. I. Seo, "Nonlinear adaptive control based on fuzzy sliding mode technique and fuzzy-based compensator," *ISA Transactions*, vol. 70, pp. 309-321, 2017.

[28] S. D. Nguyen and K. N. Ngo, "An adaptive input data space parting solution to the synthesis of neuro-fuzzy models," *Int. J. of Control, Automation, and Systems*, vol. 6, no. 6, pp. 928-938, 2008.

[29] S. D. Nguyen, S. B. Choi, and T. I. Seo, "Adaptive fuzzy sliding control enhanced by compensation for explicitly unidentified aspects," *Int. J. of Control, Auto. and Sys.*, vol. 15, pp. 2906-2920, 2017.

[30] C. Chen, B. Zhang, G. Vachtsevanos, and M. Orchard, "Machine condition prediction based on adaptive neuro-fuzzy and high-order particle filtering," *IEEE Tran. on Ind. Elec.*, vol. 58, no. 9, pp. 4353-4364, 2011.

[31] A. Ali, "Impulse noise reduction in audio signal through multi-stage technique," *Eng. Science and Tech., an Inter. J*, vol. 22, pp. 629-636, 2019.

[32] F. Ramsey, "Understanding the basis of the Kalman Filter via a simple and intuitive derivation," *IEEE Signal Pro. Mag.*, vol. 128, pp. 1-5, 2012.

[33] W. Greg and B. Gary, *An Introduction to the Kalman Filter*, UNC-Chapel Hill, TR 95-041, 2016.

[34] S. D. Nguyen, S.-B. Choi, and J.-H. Kim, "Smart dampers-based vibration control - Part 1: Measurement data processing," *Mech. System and Signal Pro.*, 2020. DOI: 10.1016/j.ymssp.2020.106958

[35] K. Cengiz, K. Cem, and T. Önsen, "A weighted mean filter with spatial-bias elimination for impulse noise removal," *Dig. Sig. Pro.*, vol. 46, pp. 164-174, 2015.

[36] P. H. Lin, B. H. Chen, S. C. Cheng, and S. C. Huang, "A morphological mean filter for impulse noise removal," *IEEE/OSA J of Display Technology*, vol. 12, no. 4, pp. 344-350, 2016.

[37] A. W. Benjamin, O. B. Kwame, and T. A. Sampson, "Efficient novel vector median filter design for impulse noise suppression in color images," *Int.t J. of Inno. Comp. Infor. and Cont.*, vol. 13, no. 6, pp. 1349-4198, 2017.

[38] C. Spinola and A. Gago, "Filtering of impulse noise from twin laser sensor signals in the process of non-contact thickness measurement in a stainless steel sheet production line," *IEEE Instr. and Mea. Tech. Conf.*, Baltimore, MD, USA, pp 1-4, 2000.

[39] L. Zhang, Y. Zhu, and W. X. Zheng, "Synchronization and state estimation of a class of hierarchical hybrid neural networks with time-varying delays," *IEEE Trans. on Neu. Net. and Learning Systems*, vol. 27, no. 2, pp. 459-470, 2016.

[40] W. Gong and Z. Cai, "Differential evolution with ranking-based mutation operators," *IEEE Trans. on Cybern.*, vol. 43, pp. 1-16, 2013.

Nang Toan Truong received his master's degree in automation engineering from Ho Chi Minh City University of Transport (UT-HCMC) in 2011. Currently, he is a Ph.D. student at Institute for Computational Science (INCOS), Ton Duc Thang University, TDTU. Also, he is a lecturer at Industrial University of Ho Chi Minh City (IUH), Vietnam. His research interests include artificial intelligence and its applications to nonlinear control, data mining, system identification, and structures' health managing.

Tae-Il Seo received his Ph.D. Degree in mechanical engineering from Ecole Centrale de Nantes, France, in 1998. From 1998 to 1999, he was a postdoctoral research fellow in the Department of Mechanical Engineering in Inha University, Incheon, Korea. From 1999 to 2001, he was a research fellow in the Department of mechanical corporation Laboratory, Inha University of Korea. From 2001 to 2003, he was a researcher in the Department of Precision Mold Lab, KITECH (Korea Institute of Industrial Technology), Korea. Currently, he is a Professor in the Department of Mechanical Engineering at Incheon National University, Korea. Dr. Seo's current research interests include micro end-milling, intelligent manufacturing system, CAD/CAD systems, etc.

Sy Dzung Nguyen received his M.E. degree in manufacturing engineering from Ho Chi Minh City University of Technology (HCMUT) - VNU in 2001 and a Ph.D. degree in applied mechanics in 2011 from HCMUT. He is an Assoc. Professor at Institute for Computational Science (INCOS), Ton Duc Thang University, Ho Chi Minh City, Vietnam. He is currently the Head of Division of Computational Mechatronics (DCME), INCOS. He was a postdoctoral fellow at Inha University, Korea in 2011-2013, at Incheon National University, Korea in 2015-2016. His research interests include artificial intelligence and its applications to nonlinear adaptive control, system identification and managing structure damage. Dr. Nguyen has been the main author of plenty of ISI papers in these fields.